ACS NANO

www.acsnano.org

ARTICLE

Ion Gel Capacitively Coupled Tribotronic Gating for Multiparameter Distance Sensing

Huai Zhang,[▽] Jinran Yu,[▽] Xixi Yang,[▽] Guoyun Gao, Shanshan Qin, Jia Sun, Mei Ding, Chuankun Jia, Qijun Sun,* and Zhong Lin Wang*

Cite This: ACS Nano 2020, 14, 3461−3468

Read Online

ACCESS | Metrics & More | Article Recommendations | Supporting Information

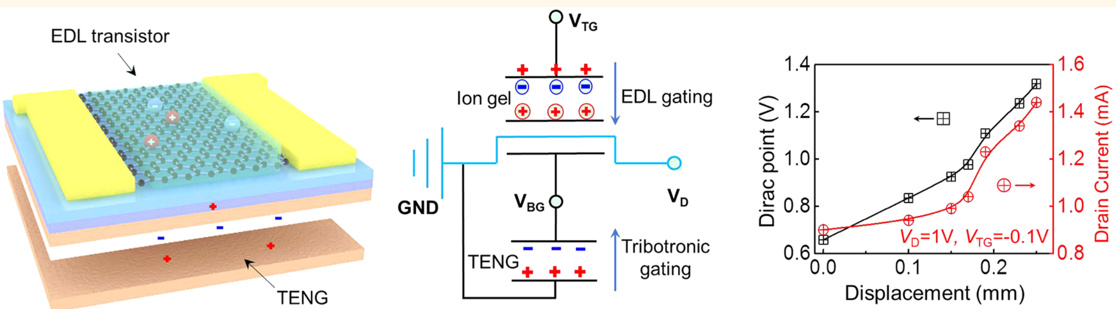

ABSTRACT: **Developing sophisticated device architectures is of great significance to go beyond Moore's law with versatility toward human−machine interaction and artificial intelligence. Tribotronics/tribo-iontronics offer a direct way to controlling the transport properties of semiconductor devices by mechanical actions, which fundamentally relies on how to enhance the tribotronic gating effect through device engineering. Here, we propose a universal method to enhance the tribotronic properties through electric double layer (EDL) capacitive coupling. By preparing an ion gel layer on top of tribotronic graphene transistor, we demonstrate a dual-mode field effect transistor (*i.e.*, a tribotronic transistor with capacitively coupled ion gel and an ion-gel-gated graphene transistor with a second tribotronic gate). The resulted tribotronic gating performances are greatly improved by twice for the on-state current and four times for the on/off ratio (the first mode). It can also be utilized as a multiparameter distance sensor with drain current increased by ∼600 μA and threshold voltage shifted by ∼0.8 V under a mechanical displacement of 0.25 mm (the second mode). The proposed methodology of EDL capacitive coupling offers a facile and efficient way to designing more sophisticated tribotronic devices with superior performance and multifunctional sensations.**

KEYWORDS: *tribotronic gating, capacitive coupling, ion gel, distance sensing, graphene*

Field effect transistors (FETs) are the cornerstones of modern IT industry,[1−4] which have made great contributions in integrated circuits,[5] nonvolatile memory,[6] advanced electronic/optoelectronic sensors,[7] and neuromorphic devices.[8] Si transistors are approaching the scaling technology node of ∼3 nm due to the short channel effect, loss of electrostatic gate modulation, and arising source-to-drain tunneling current issue.[9] Except the exploration of high performance channel materials (*e.g.*, two-dimensional semiconductors in atomic thickness possessing the advantage of larger band gap, lower dielectric constant and heavier carrier mass),[10] to develop sophisticated device architectures is also of significant meaning to go beyond Moore's law with diversity and versatility toward human−machine interface and artificial intelligence. Since the invention of triboelectric nanogenerator (TENG),[11] it is highly promising for low-frequency mechanical energy scavenging, specific micro/high-voltage power sources, and motivating the self-powered systems in the era of Internet of Things,[12−15] which also encourages the potential integrations of distributed energy harvesting and distributed energy storage to emerge from the horizon.[16−18] An interdisciplinary research field has also emerged by coupling the triboelectric potential with semiconductor devices, *i.e.*, tribotronics[19] and tribo-iontronics.[20] It delivers a direct and effective way of controlling the electrical transport properties of the semiconductor devices by using external mechanical actions. The

Received: December 5, 2019
Accepted: February 14, 2020
Published: February 14, 2020

https://dx.doi.org/10.1021/acsnano.9b09549
ACS Nano 2020, 14, 3461−3468

tribotronic or tribo-iontronic devices are capable of working as phototransistors,[21] tunable logic devices,[22] and memory[23] and tactile sensors,[24−26] which also further the development of artificial intelligence[27−29] and neuromorphic devices.[30] In fact, the intrinsic working mechanism of the tribotronic devices is to control the output currents by the displacement of integrated TENG. Hence, the displacement derived characterizations with corresponding figures of merit are critical for the development of tribotronic devices, *e.g.*, tribotronic transconductance (∼μA·μm^{-1}), tribotronic threshold displacement (∼μm), tribotronic subthreshold swing (∼μm/dec), *etc.*[20]

Previous research mainly focused on the diversified and multifunctional applications of tribotronic FET. Some important parameters, such as on/off ratio, cutoff current, and threshold displacement have not been further optimized. To achieve advanced tribotronic devices with superior electrical performances and more efficient tribotronic gating control capacity, the key point is to minimize the required triboelectric potential (related with TENG displacement) for unit output current variation, which can be evaluated by displacement per decade (∼μm/dec). Dual-gate tribotronic FET[22] has been utilized to achieve high performance tribotronic gating efficacy and realize displacement-tunable properties. Solid-state electrolyte[31−33] is another optional dielectric layer to reduce the operating gate voltage due to the formation of electrical double layers (EDLs, with an ultrahigh capacitance of ∼ μF·cm^{-2}) during the working process.[34,35] Taking advantage of the ultrahigh capacitive EDLs in the dual-gate transistor architecture may lead to more efficient capacitive coupling effect to significantly reduce the commonly required high operating gate voltage and improve the tribotronic gating performances.[36] Meanwhile, the dual-gate architectures[37] introduces the tribo-electrostatic modulation on the charge carrier distribution accumulated by the first gate, which delivers larger space to design more sophisticated multiparameter distance sensor for noncontact sensations.

In this work, we propose a universal method to enhance the tribotronic gating effect through ion gel capacitive coupling (*i.e.*, intrinsically, ultrahigh capacitive coupling through EDLs). By preparing an ion gel layer on top of the tribotronic graphene transistor on SiO_2/Si wafer, we fabricate a dual-mode field effect transistor. One mode can be considered as a tribotronic transistor with capacitively coupled ion gel to enhance the modulation capacity of triboelectric potential. The other mode is from the aspect of an ion-gel-gated graphene transistor with a second tribotronic gate for distance sensor. Based on the capacitive coupling of ion gel, the tribotronic electric performance is greatly improved (the first mode). The corresponding on-state current increases by twice and on/off ratio increases by four times. According to the introduction of tribotronic dual-gate, the ion-gel-gated transistor (the second mode) can be utilized as a highly sensitive multiparameter distance sensor (drain current and threshold voltage). When the TENG displacements change by 0.25 mm, the channel current dramatically increases by ∼600 μA and the threshold voltage shifts by ∼0.8 V. The demonstrated methodology of EDL capacitive coupling boosts the triboelectric potential gating properties, offering a facile and efficient way to designing more sophisticated tribotronic devices with superior performance and multifunctional sensations. It is also promising to be applicable to electronic skin sensors, noncontact distance sensor, human-computer interactive devices, *etc.*

RESULTS AND DISCUSSION

Figure 1a shows the schematic illustration of the dual-mode FET, including the EDL transistor and tribotronic transistor

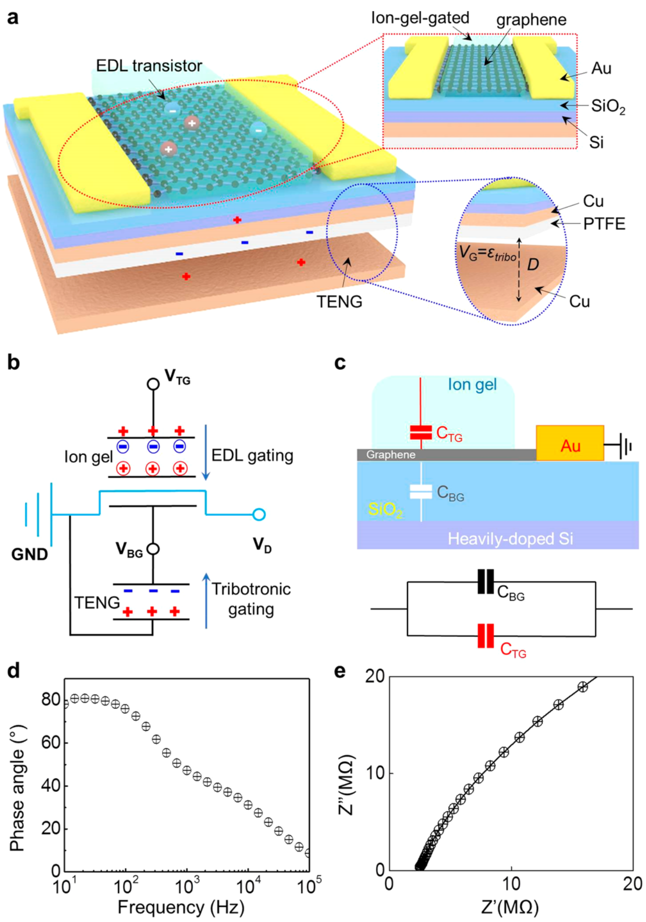

Figure 1. (a) Schematic illustration of the dual-mode FET. (b) Corresponding circuit diagram of the dual-mode FET. (c) Schematic illustration of the connected capacitors and equivalent circuit diagram. (d) Phase angle of ion gel capacitor as a function of the applied frequency. (e) Impedance analysis, Nyquist plot.

distinguished by different gate dielectrics. The first mode is a tribotronic transistor gated by triboelectric potential originated from the bottom TENG. The top ion gel offers a EDL capacitive coupling effect to enhance the tribotronic modulation performance (top inset of Figure 1a). The other mode of the EDL transistor can be regarded as an ion-gel-gated graphene transistor with a second tribotronic gate (*i.e.*, dual-gate transistor, bottom inset of Figure 1a). The output current and threshold voltage can be modulated by the triboelectric potential, which is determined by the displacement of TENG. Hence, the EDL transistor can work as a distance sensor. The corresponding circuit diagram of the dual-mode FET is shown in Figure 1b.

In the dual-mode FET, the *p*-type doped Si with 300 nm thick SiO_2 film is used as the supporting substrate and gate dielectrics for tribotronic gating. The top gate dielectrics is a solid-state electrolyte, *i.e.*, an ion gel with ultrahigh capacitance (>1 μF·cm^{-2}) due to the EDLs formation during working

https://dx.doi.org/10.1021/acsnano.9b09549
ACS Nano 2020, 14, 3461−3468

process. Graphene grown by chemical vapor deposition (CVD) is utilized as the channel of the dual-mode transistor, patterned on SiO_2/Si substrate after standard wet transfer and photolithography processes. The Raman spectrum of the graphene channel is shown in Figure S1. The sharp G peak and 2D peak at 1580 and 2700 cm^{-1} with peak value ratio (I_G/I_{2D}) below 1/2 indicate that the graphene used in the experiment is monolayer. The unconspicuous D peak represents the high quality of the CVD grown graphene.[38] Cr/Au (10 nm/40 nm) thin films deposited by thermal evaporation are used as source−drain electrodes. The bottom triboelectric potential gating is originated from the integrated TENG, comprising of the polytetrafluoroethylene (PTFE) electrification layer sandwiched by two Cu electrodes in a typical contact-separation mode. The top gate of the ion gel is precisely patterned on the graphene channel, which is composed of ion liquid (1-ethyl-3-methylimidazolium bis-(trifluoromethylsulfonyl)imide ([EMIM][TFSI]) and photo-cross-linked polymer. In the dual-gate geometry, capacitive coupling between the bottom and top gate dielectrics can cause the effective capacitance to deviate significantly from the nominal parallel-plate value. As the patterned ion gel does not contact with the Au source−drain electrodes (Figure S2), schematic illustration of the connected capacitors is shown in Figure 1c. Both the EDLs formed at the ion gel/graphene interface (capacitance defined as C_{TG}) and the intrinsic SiO_2 dielectrics (C_{BG}) contribute to the effective capacitance. The equivalent circuit diagram is shown at the bottom of Figure 1c. The triboelectric potential originated from the TENG component is applied to the effective capacitor between Au and the heavily doped Si, which can be simplified as C_{TG} and C_{BG} connected in parallel. In this system, the relationship between the effective capacitance and each capacitive part can be described by the following equation:[36]

$$C = C_{TG} + C_{BG}$$

As $C_{TG} \gg C_{BG}$, when the two gates of the transistor are working simultaneously, the effective capacitance (C_{eff}) is approximately equal to C_{TG}. Thus, even the first tribotronic transistor mode works through SiO_2 dielectrics and the triboelectric potential can be considered to couple to the graphene channel through an ultrahigh capacitance (similar to EDLs capacitance), resulting in an enhanced tribotronic gating effect by the ion gel capacitive coupling. The corresponding phase angle of the ion gel capacitor as a function of the applied frequency is shown in Figure 1d. At low frequency, the phase angle of the polarized ion gel is close to 90°, indicating that the effective capacitance of the system is high. This capacitance characteristic is mainly due to the formation of EDLs. The Nyquist plot shows that the steep slope in the low frequency region exceeds 1 (Figure 1e). This indicates that the ion gel derived EDLs capacitor can store a large amount of charges, which endows an adjustable capacity of charge carriers transport in the transistor channel. The dielectric properties of the ion gel are also characterized by $C-V$ measurement with a metal−insulator−semiconductor (MIS) structure covered with ion gel. The specific capacitance of the device increases with the absolute value of the applied bottom gate voltage (−2 to +2 V, Figure S3), which is attributed to the accumulation of ions at the ion gel/graphene channel interface to form EDLs under positive/negative gate bias. The maximum effective capacitance reaches 8.3 $\mu F \cdot cm^{-2}$, which is much larger than the capacitance of traditional dielectric layers (*e.g.*, 11.5 $nF \cdot cm^{-2}$ for 300 nm SiO_2 dielectrics).

The basic output performance of the bottom gate graphene transistor without ion gel is shown in Figure 2a. The output

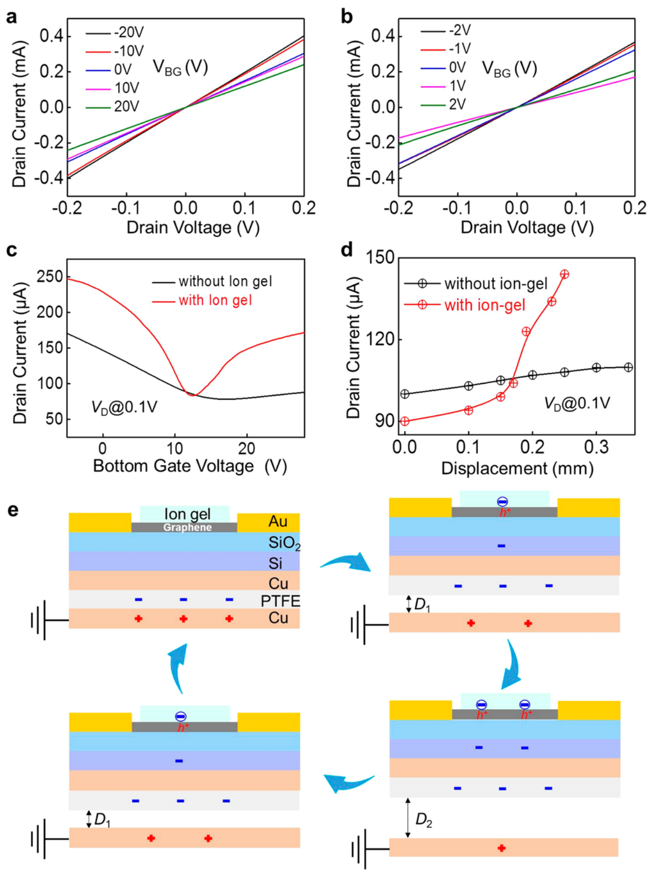

Figure 2. Typical output performance of the bottom gate graphene transistor (a) without ion gel and (b) with top ion gel. (c) Transfer curves of the graphene transistor with/without top ion gel. (d) Corresponding tribotronic transfer curves. (e) Working mechanism for the first mode of tribotronic transistor.

drain current (I_D) increases from 0.24 to 0.41 mA with the bottom gate voltage (V_{BG}) applied from +20 to −20 V at a drain voltage (V_D) of 0.2 V. For the graphene transistor with top ion gel, the applied V_{BG} is greatly decreased from −20 to −2 V to achieve a similar I_D output at 0.4 mA (at V_D = 0.2 V, Figure 2b). The required V_{BG} is decreased by ten times according to the ion gel capacitive coupling effect; *i.e.*, the effective capacitance of this device is in the level of ∼ $\mu F \cdot cm^{-2}$ similar to the EDL device. When we apply the V_{BG} of −20 V to the ion gel coupled device, the I_D increases to approach 1 mA (inset of Figure S4). Figure 2c shows that the transfer curves of the graphene transistor with and without top ion gel are vastly different. In the absence of top ion gel, the transfer curve of graphene is smooth with a low on/off current ratio ($I_{on/off}$ = 1.5). The ambipolarity of graphene is not obvious with the Dirac point (V_{Dirac}) at 17 V and the output current is relatively low (170 μA) at a gate voltage (V_G) of −5 V. In contrast, the graphene transistor with ion gel shows a steeper transfer curve. Both the ambipolar transport properties and on/off current ratio are improved. The V_{Dirac} is decreased to 12 V and the $I_{on/off}$ increases to 3. The extracted field effect mobility of the ion gel coupled graphene transistor is also improved from ∼7

https://dx.doi.org/10.1021/acsnano.9b09549
ACS Nano 2020, 14, 3461−3468

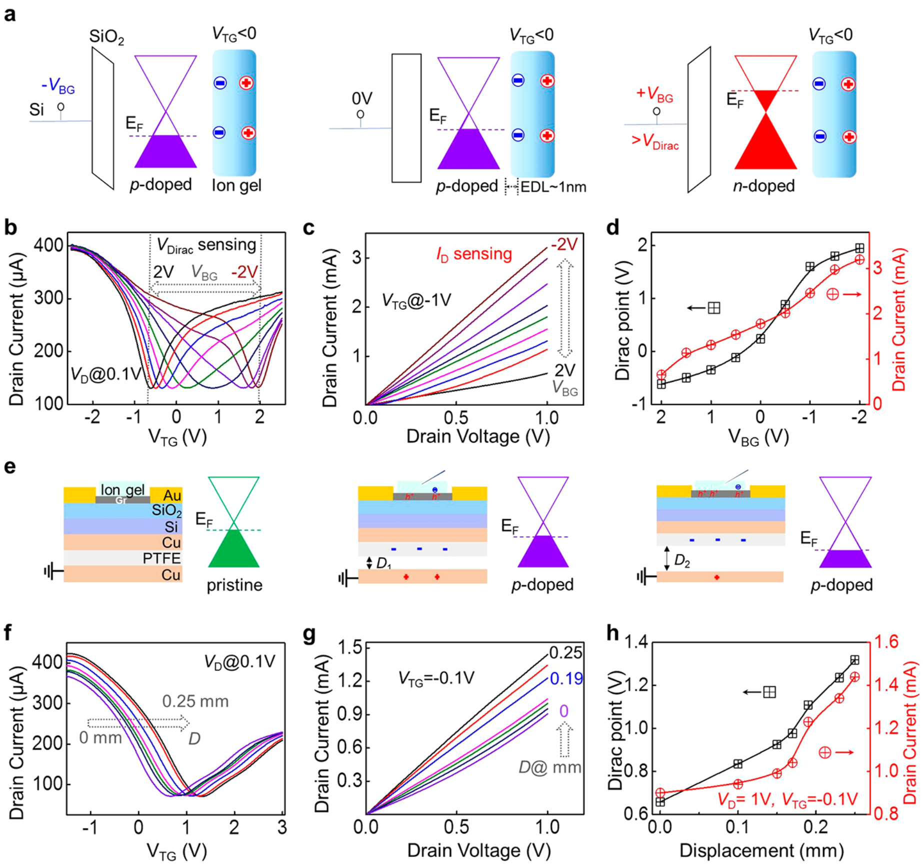

Figure 3. (a) Energy band diagrams of the ion-gel-gated graphene FET under negative V_{TG} with applied different V_{BG}'s. (b) Typical transfer curves and (c) output curves of the dual-gate graphene transistor. (d) Extracted V_{Dirac} and I_D *vs* V_{BG}. (e) Working principle and energy band diagram of the device in the second mode. (f) Typical transfer curves and (g) output curves of the ion-gel-gated graphene transistor with a second tribotronic gate. (h) Extracted V_{Dirac} and I_D *vs* *D*.

to ~100 $cm^2 \cdot V^{-1} \cdot s^{-1}$ for the holes transport and from 40 to 154 $cm^2 \cdot V^{-1} \cdot s^{-1}$ for the electrons transport (extracted from Figure 2c, V_G sweeps from −5 to 30 V). The field effect mobility of graphene transistor gating with only top ion gel or bottom SiO_2 are also characterized in Figure S5. Besides, if a second gate voltage is applied through top ion gel gate (−0.2 to 0.2 V) under the sweeping of bottom gate, the transfer curves exhibit typical stepped shifts with varied V_{Dirac}'s (Figure S6).

Figure 2d shows the corresponding transfer curves (I_D *vs* displacement) of the tribotronic graphene transistor. When there is no ion gel, tribotronic gating effect with TENG displacement from 0 to 0.3 mm is very weak (almost no on/off ratio) due to the relatively low capacitance of SiO_2. The tribotronic potential at TENG displacement of 0.3 mm is not sufficient to modulate the Fermi level of graphene. For the ion gel covered device, I_D obviously increases from 90 to 144 μA at V_D = 0.1 V under the same TENG displacement. All of the above results demonstrate the coupled top ion gel enables more efficient control of the channel current through the bottom SiO_2 gate. For the first mode of tribotronic transistor, the working mechanism is shown in Figure 2e. The Cu/PTFE/Cu-TENG component supplies the triboelectric potential as the equivalent gate voltage to the graphene transistor. The top patterned ion gel offers the capacitive coupling means to enhance the tribotronic gating performance. At the initial state, the movable Cu electrode contacts with the PTFE. The induced opposite electrostatic charges are balanced with each other. No triboelectric potential is applied to the graphene transistor. When the Cu electrode starts to separate from the PTFE (D_1), the induced negative charges on PTFE cannot be fully neutralized by the positive charges on Cu, which leads to an equivalent negative gate voltage applied to the graphene channel and dominates the holes transport. With the separation distance further increasing, more negative charges contribute to the triboelectric potential gating on graphene channel to increase the output current. When the Cu electrode moves back, the induced negative electrostatic charges on PTFE are reneutralized gradually, leading to a decreased triboelectric potential gating until they fully contact with each other (V_{TENG} = 0 V). The output voltage of the integrated TENG component according to the displacement is shown in Figure S7, which can provide 0 to 8 V working voltage to drive the graphene transistor. The extracted figure of merits of the tribotronic graphene transistor is 216 $\mu A \cdot mm^{-1}$ for the tribotronic transconductance, and 0.67 $mm \cdot dec^{-1}$ for the tribotronic subthreshold swing.

For the second mode of ion-gel-gated transistor on SiO_2/Si, we first explain its working principle and investigate the basic electrical performances. Figure 3a shows the energy band diagrams of the ion-gel-gated graphene FET under negative top gate voltage (V_{TG}) with applied different V_{BG}s. When a negative V_{TG} is applied through the ion gel with V_{BG} = 0 V, the cations are attracted to the gate side, while the anions are repelled to the graphene channel side. EDLs are induced at the gate/ion gel and graphene/ion gel interfaces, respectively. The

https://dx.doi.org/10.1021/acsnano.9b09549
ACS Nano 2020, 14, 3461−3468

Fermi level of graphene is shifted downward with holes dominating the transport properties of the graphene channel in this state (middle panel of Figure 3a). When a negative V_{BG} is applied under the same V_{TG}, both of the negative gate voltages influence graphene Fermi level to further shift downward (left panel of Figure 3a). The negative V_{BG} induces a further electrostatic *p*-type doping in graphene channel through the bottom gate. In this state, the holes continue to dominate the transport in graphene channel. In contrast, when a positive V_{BG} is applied under the same V_{TG}, there will be two different cases because positive V_{BG} contributes to an *n*-type doping in graphene channel. As show in the right panel of Figure 3a, when the V_{BG} is positive and larger than the Driac voltage ($+V_{BG} > V_{Dirac}$), the V_{BG}*n*-type doping effect will exceed the V_{TG}*p*-type doping effect. The Fermi level of graphene is shifted upward across the Dirac point with electrons dominating the charge transport. If the applied positive $V_{BG} < V_{Dirac}$, (Figure S8a), the V_{BG} *n*-type doping effect cannot suppress the V_{TG}*p*-type doping effect. The Fermi level of graphene will still locate below the Dirac point with holes dominating the charge transport. The energy band diagrams of the EDL graphene transistor under positive V_{TG} are discussed in Figure S8b,c.

Typical transfer curves of the dual-gate graphene transistor are shown in Figure 3b. According to the electrostatic doping on graphene through the bottom gate, the transfer characteristics are tunable and represent obvious shifts under different V_{BG}s. At V_{BG} = 0 V, the transfer curve shows ambipolar transport properties with V_{Dirac} located at 0.24 V (green curve in Figure 3b). The applied negative/positive V_{BG} induces typical *p*-/*n*-type doping in the graphene channel, which shifts the V_{Dirac} to the positive/negative gate voltage direction. When the applied V_{BG} decreases from +2 to −2 V, the V_{Dirac} represents a clear shift from −0.62 to +1.95 V (black curve in Figure 3d). If we replace the applied V_{BG} with triboelectric potential, which is determined by TENG displacement (D), the V_{TG} region (ranged from −0.62 to +1.95 V) can be considered as a V_{Dirac} sensitive region and used for distance sensing. In the V_{TG} regions beyond V_{Dirac}-sensitive region (<0.62 V and >1.95 V), I_D represents a clear unidirectional variation, indicating these two regions are D-dependent I_D-sensitive regions. Considering that holes transport is superior compared with electrons, we take V_{TG} at −1 V as an example. Corresponding output curves under different applied V_{BG}s are shown in Figure 3c. I_D increases from 0.64 to 3.2 mA with V_{BG} decreased from +2 to −2 V (red curve in Figure 3d). Hence, the second mode of ion-gel-gated transistor with bottom tribotronic gating (related with TENG displacement D) has potential to be utilized as a multiparameter distance sensor (V_{Dirac} and I_D as the sensing parameters, respectively). Notably, the applied V_{BG}s to achieve the tunable properties are greatly decreased to the level of <2 V even though they are applied through the SiO_2 dielectrics. This is a benefit owing to the capacitive coupling between SiO_2 and ion gel, which can assist to achieve analogous tribotronic gating performance in high efficiency.

For the distance sensing test of the second mode transistor (ion-gel-gated graphene transistor with the bottom tribotronic gating), the TENG (Cu/PTFE/Cu) is integrated on the bottom of Si wafer. The applied V_{BG} is totally replaced with the triboelectric potential induced by the displacement of TENG. Figure 3e shows the corresponding working principle and energy band diagram of the device in the second mode. For better comprehension, we take the state of V_{TG} at 0 V as an example. At the initial stage, the Cu electrode fully contacts with the PTFE. No triboelectric potential is induced to gate the transistor. The Fermi level of graphene is slightly downward shifted due to the *p*-type doping of graphene by the oxygen/moisture in atmospheric environment. When the Cu separates from PTFE for a certain distance, the unbalanced tribo-electrostatic charges induce an equivalent negative V_{BG} to the transistor. It induces tribo-electrostatic *p*-type doping to the graphene channel and shifts the Fermi level of graphene downward. Under the continuous separation between Cu and PTFE, the enhanced positive triboelectric potential results in the aggravated tribo-electrostatic doping in graphene channel, which further shift the graphene Fermi level downward. The transfer curves of the ion-gel-gated transistor with extra tribotronic gating are recorded in Figure 3g, exhibiting effective shifts under different displacements. The corresponding output performances under different displacements are shown in Figure 3f. The extracted V_{Dirac} and I_D shift from 0.6 to 1.4 V and from 0.9 to 1.44 mA with the displacement increased from 0 to 0.25 mm, respectively (at V_D = 1 V, V_{TG} = −0.1 V, Figure 3h). Another group of V_{Dirac} and I_D extracted from Figure 3g is shown in Figure S9 to supplement the sensing properties of the graphene transistor at V_D = 0.1 V (V_{TG} = 0 V for holes-dominating transport region and V_{TG} = 2 V for electrons-dominating transport region). The sensing current level (100 to 300 μA) is similar to that in Figure 2d (~100 μA). From the aspect of distance sensor, the achieved I_D and V_{Dirac} can be considered as a function of TENG displacement, *i.e.*, the displacement induces the variations of both I_D and V_{Dirac}. Hence, the second mode of ion-gel-gated transistor with bottom tribotronic gating can be utilized as a multiparameter distance sensor. Furthermore, the V_{TG}, serving as the "top gating state", is variable and definable, which can introduce tunable sensitivity in the multiparameter distance sensing process. Under different V_{TG}'s, the sensitivity of the distance sensor can be tuned, which is very important for the users to select specific V_{TG} according to different application circumstances.

Prior to the research on the tunable sensitivity of the distance sensor based on the ion-gel-gated graphene transistor with tribotronic gating, we extract the ΔI_D *vs* V_{BG} at the I_D sensitive region (V_{TG} ranged from −2 to −1 V) from Figure 3c. Thereinto, ΔI_D is defined as the current difference between the I_D at a certain V_{BG} ($\neq 0$) and the I_D at V_{BG} = 0 V. The extracted curves are plotted in Figure 4a. The derivative of each curve ($\Delta I_D/V_{BG}$) is further extracted as shown in Figure 4b, the physical meaning of which is the volume of the I_D variation induced by the second tuning gate V_{BG} (relative to the driving gate V_{TG} through ion gel). From Figure 4b, it is observed that I_D shows the largest variation at a V_{TG} of −1 V, which means V_{TG} at −1 V will give rise to the highest sensitivity. Analogously, for the ion-gel-gated graphene transistor with tribotronic gating, the ΔI_D *vs* displacements at different V_{TG}'s have also been extracted at the I_D-sensitive region (V_{TG} ranged from −1 to 0 V) from Figure 3g. Corresponding relations between ΔI_D and D are shown in Figure 4c. The slope of each curve ($\Delta I_D/D$) is also extracted (Figure 4d), which is an evaluation of the capacity of I_D variation according to the TENG displacement. From the curve, it can be concluded that the V_{TG} at 0 V enables the multiparameter distance sensor to achieve the highest sensitivity in this work. Besides, ΔI_D *vs* D of the bottom tribotronic graphene transistor without ion gel is shown in

https://dx.doi.org/10.1021/acsnano.9b09549
ACS Nano 2020, 14, 3461−3468

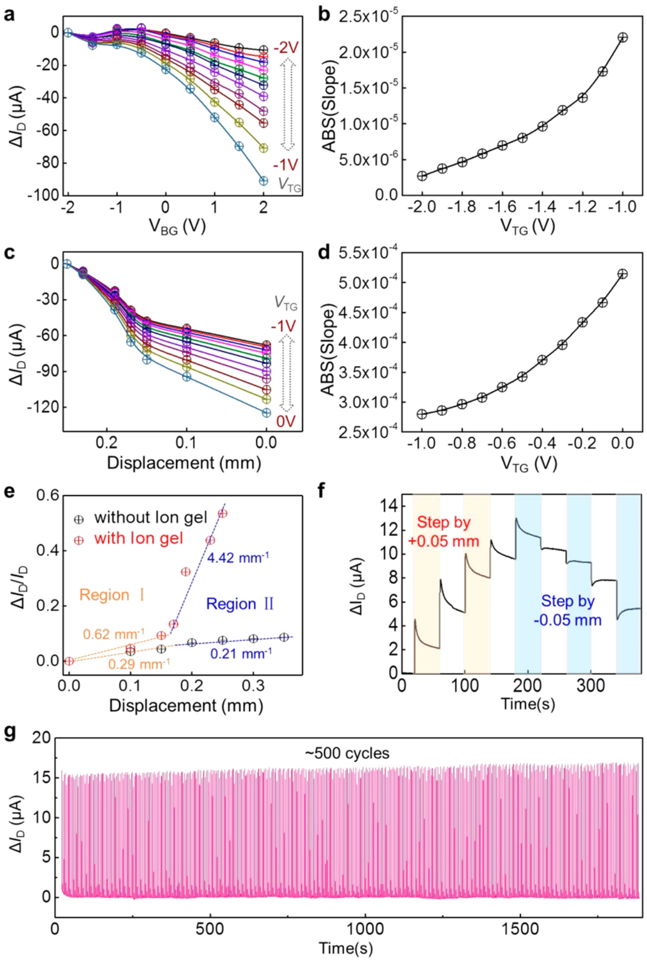

Figure 4. (a) Extracted ΔI_D *vs* V_{BG} at the I_D sensitive region (V_{TG} ranged from −2 to −1 V) and (b) the slope of each curve ($\Delta I_D/V_{BG}$). (c) Extracted ΔI_D *vs* D at the I_D sensitive region (V_{TG} rangedfrom −1 to 0 V) and (d) slope of each curve ($\Delta I_D/D$). (e) Sensitivity of the distance sensor, normalized $\Delta I_D/I_D$ *vs* D. (f) Real-time distance sensing test. (g) Durability and long-term stability distance sensing test.

Figure S10 to confirm the ion gel capacitive coupling is valid for improving the sensitivity of the distance sensor. The ΔI_D achieved with ion gel is obviously higher than that achieved without ion gel. The normalized $\Delta I_D/I_D$ *vs* D (the slope of the curve is commonly defined as the sensitivity) is also shown in Figure 4e, exhibiting a similar variation trend with the counterparts under both applied V_{TG} and V_{BG}. The sensitivity of ion-gel-gated distance sensor is 0.62 mm^{-1} and 4.42 mm^{-1} in region I and II, respectively, which is much higher than the tribotronic distance sensor without ion gel (0.29 mm^{-1} and 0.21 mm^{-1}). The above results confirm that the second mode of ion-gel-gated transistor with bottom tribotronic gating can be qualified as a highly efficient, tunable, and multiparameter distance sensor.

Figure 4f shows the real-time distance sensing test of the multiparameter graphene transistor. The output current variation increases steppedly from 0 to 12 μA with the increased displacement of TENG component from 0 to 0.25 mm (stepped by 0.05 mm). The ΔI_D value is determined by the electrostatic doping level of graphene channel induced by the coupled bottom-gate triboelectric potential. The extracted forward and afterward response time is ~0.2 s (Figure S11a). In contrast, under the same stepped displacements, ΔI_D of the tribotronic graphene transistor without ion gel is only increased from 0 to 4 μA (three times lower than the multiparameter distance sensor) due to the lack of EDL capacitive coupling (Figure S11b). The maintainability of the sensing signals is critical for the distance sensor in practical applications. As shown in Figure S11c, when the displacement is increased to 0.001 and 0.005 mm and then maintained for certain time, the distance sensor responses fast with the output sensing signal increased to 420 and 440 μA and remains stable for over 60 s. The excellent maintainability of the distance sensor is attributed to the low bottom gate leakage current (<0.1 nA), which ensures the highly efficient tribotronic gating properties. The durability and long-term stability tests are also conducted to the distance sensor (Figure 4g). The ΔI_D peaks can be maintained stable at ~15 μA over 500 cycles of contact-separation distance sensing tests (displacement at 0.25 mm). The effective, fast, and stable distance sensing by the multiparameter graphene transistor is originated from the ion gel capacitive coupling enhanced tribotronic gating effect, which is promising for practical noncontact sensors, human-machine interactive devices, intelligent robotic sensing applications, *etc.*

CONCLUSION

In summary, an effective method to enhancing the tribotronic gating effect through ion gel capacitive coupling has been proposed. The demonstrated dual-mode FET owing to the introduction of EDL capacitive coupling successfully accomplishes the high performance tribotronic gating (the first mode) and multiparameter distance sensing (the second mode). By coupling the top ion gel, the on-state current of the dual-mode FET increases by twice, the on/off ratio increases by four times and the field effect mobility increases by ten times. Furthermore, multiparameter distance sensation is realized relying on the output current and threshold voltage. The proposed EDL capacitive coupling is a universal method to boosting the triboelectric potential gating properties and reducing device power consumption, which may also promote the development of more sophisticated tribotronic sensing devices. The demonstrated dual-mode tribotronic graphene FET is believed to enable inspirations of more diversified and versatile functional devices to go beyond Moore's law.

METHODS

Device fabrication: A 10/50 nm Cr/Au electrode was deposited on the *p*-type doped Si with 300 nm thick SiO_2 film using a thermal evaporation system. The coplanar gate, source and drain electrodes were formed by typical photolithography (photoresist AZ5214) and acid etching process. High-quality monolayer graphene was grown on the surface of the copper catalyst using CVD, confirmed by Raman spectrum. It was transferred on SiO_2/Si wafer through the standard wet transfer process and patterned using photolithography and reactive ion etching (RIE, Si 500, SENTECH Instruments GmbH). The graphene channel length and width are 10 and 100 μm, respectively. The UV-curable ionic gel was also photopatterned on top of the graphene channel and a portion of the Au gate electrode to form the top gate dielectrics. Ionic gel composed of [EMIM][TFSI] ionic liquid, polyethylene glycol diacrylate (PEGDA) monomer and 2-hydroxy-2-methylacetophenone (HOMPP) photoinitiator is in the weight ratio of 90:7:3. TENG composed of Cu/PTFE/Cu structure in contact-separation mode was integrated to the bottom Si gate of the graphene FET.

https://dx.doi.org/10.1021/acsnano.9b09549
ACS Nano 2020, 14, 3461−3468

Performance characterization: TENG output performance was measured with the electrometer Keithley 6514. Electrical performances of graphene FETs were measured with a semiconductor analysis system, Keysight Agilent B1500A. The ion gel capacitance characterization was conducted by an impedance analyzer, Agilent E4900A.

ASSOCIATED CONTENT

Supporting Information

The Supporting Information is available free of charge at https://pubs.acs.org/doi/10.1021/acsnano.9b09549.

> Raman spectroscopy of the CVD grown graphene; photo image of the channel length and width of graphene FET; specific effective capacitance *vs* the applied bottom gate voltage; output performance of the bottom gate graphene transistor with ion gel under V_{BG} from −20 to +20 V; transfer curves of the graphene transistor under top and bottom gate voltage; transfer curves of graphene transistor with a second gate voltage applied from top ion gel gate from −0.2 to +0.2 V; TENG output voltage *vs* displacement; energy band diagrams of the EDL graphene transistor under negative V_{TG}; another group of V_{Dirac} and I_D extracted from Figure 3g; ΔI_D *vs* D of the bottom tribotronic graphene transistor without ion gel; real-time distance sensing test of the graphene transistor (PDF)

AUTHOR INFORMATION

Corresponding Authors

Qijun Sun − *Beijing Institute of Nanoenergy and Nanosystems, Chinese Academy of Sciences, Beijing 100083, China; School of Nanoscience and Technology, University of Chinese Academy of Sciences, Beijing 100049, China; Center on Nanoenergy Research, School of Physical Science and Technology, Guangxi University, Nanning 530004, China;* orcid.org/0000-0003-2130-7389; Email: sunqijun@binn.cas.cn

Zhong Lin Wang − *Beijing Institute of Nanoenergy and Nanosystems, Chinese Academy of Sciences, Beijing 100083, China; School of Nanoscience and Technology, University of Chinese Academy of Sciences, Beijing 100049, China; School of Materials Science and Engineering, Georgia Institute of Technology, Atlanta, Georgia 30332-0245, United States;* orcid.org/0000-0002-5530-0380; Email: zhong.wang@mse.gatech.edu

Authors

Huai Zhang − *Beijing Institute of Nanoenergy and Nanosystems, Chinese Academy of Sciences, Beijing 100083, China; School of Nanoscience and Technology, University of Chinese Academy of Sciences, Beijing 100049, China*

Jinran Yu − *Beijing Institute of Nanoenergy and Nanosystems, Chinese Academy of Sciences, Beijing 100083, China; School of Nanoscience and Technology, University of Chinese Academy of Sciences, Beijing 100049, China*

Xixi Yang − *Beijing Institute of Nanoenergy and Nanosystems, Chinese Academy of Sciences, Beijing 100083, China; School of Nanoscience and Technology, University of Chinese Academy of Sciences, Beijing 100049, China*

Guoyun Gao − *Beijing Institute of Nanoenergy and Nanosystems, Chinese Academy of Sciences, Beijing 100083, China; School of Nanoscience and Technology, University of Chinese Academy of Sciences, Beijing 100049, China*

Shanshan Qin − *Beijing Institute of Nanoenergy and Nanosystems, Chinese Academy of Sciences, Beijing 100083, China; School of Nanoscience and Technology, University of Chinese Academy of Sciences, Beijing 100049, China*

Jia Sun − *School of Physics and Electronics, Central South University, Changsha 410083, China;* orcid.org/0000-0003-4423-8128

Mei Ding − *College of Materials Science and Engineering, Changsha University of Science & Technology, Changsha 410114, China*

Chuankun Jia − *College of Materials Science and Engineering, Changsha University of Science & Technology, Changsha 410114, China*

Complete contact information is available at: https://pubs.acs.org/10.1021/acsnano.9b09549

Author Contributions

∇H.Z., J.Y., and X.Y. contributed equally.

Notes

The authors declare no competing financial interest.

ACKNOWLEDGMENTS

This work is financially supported by the National Key Research and Development Program of China (2016YFA0202703, 2016YFA0202704), National Natural Science Foundation of China (51605034, 51711540300), CAS Pioneer Hundred Talents Program, Beijing Nova Program (Z191100001119047), and the State key laboratory of precision measuring technology and instruments (Tianjin University).

REFERENCES

(1) Koezuka, H.; Tsumura, A.; Ando, T. Field-Effect Transistor with Polythiophene Thin Film. *Synth. Met.* **1987**, *18*, 699−704.

(2) Dennard, R. H.; Gaensslen, F. H.; Rideout, V. L.; Bassous, E.; LeBlanc, A. R. Design of Ion-Implanted MOSFET's with Very Small Physical Dimensions. *IEEE J. Solid-State Circuits* **1974**, *9*, 256−268.

(3) Waldrop, M. M. The Chips are Down for Moore's Law. *Nature* **2016**, *530*, 144.

(4) Qian, C.; Kong, L.-a.; Yang, J.; Gao, Y.; Sun, J. Multi-Gate Organic Neuron Transistors for Spatiotemporal Information Processing. *Appl. Phys. Lett.* **2017**, *110*, 083302.

(5) Kim, D.-H.; Ahn, J.-H.; Choi, W. M.; Kim, H.-S.; Kim, T.-H.; Song, J.; Huang, Y.; Liu, Z.; Lu, C.; Rogers, J. A. Stretchable and Foldable Silicon Integrated Circuits. *Science* **2008**, *320*, 507−511.

(6) Qian, C.; Sun, J.; Kong, L.-A.; Fu, Y.; Chen, Y.; Wang, J.; Wang, S.; Xie, H.; Huang, H.; Yang, J.; Gao, Y. Multilevel Nonvolatile Organic Photomemory Based on Vanadyl-Phthalocyanine/Para-Sexiphenyl Heterojunctions. *ACS Photonics* **2017**, *4*, 2573−2579.

(7) Wang, J.; Chen, Y.; Kong, L.-A.; Fu, Y.; Gao, Y.; Sun, J. Deep-Ultraviolet-Triggered Neuromorphic Functions in In-Zn-O Phototransistors. *Appl. Phys. Lett.* **2018**, *113*, 151101.

(8) Kong, L.-A.; Sun, J.; Qian, C.; Fu, Y.; Wang, J.; Yang, J.; Gao, Y. Long-Term Synaptic Plasticity Simulated in Ionic Liquid/Polymer Hybrid Electrolyte Gated Organic Transistors. *Org. Electron.* **2017**, *47*, 126−132.

(9) Lundstrom, M. Moore's Law Forever? *Science* **2003**, *299*, 210−211.

(10) Nourbakhsh, A.; Zubair, A.; Sajjad, R. N.; Tavakkoli K. G., A.; Chen, W.; Fang, S.; Ling, X.; Kong, J.; Dresselhaus, M. S.; Kaxiras, E.; Berggren, K. K.; Antoniadis, D.; Palacios, T. MoS_2 Field-Effect Transistor with Sub-10 nm Channel Length. *Nano Lett.* **2016**, *16*, 7798−7806.

(11) Fan, F.-R.; Lin, L.; Zhu, G.; Wu, W.; Zhang, R.; Wang, Z. L. Transparent Triboelectric Nanogenerators and Self-Powered Pressure Sensors Based on Micropatterned Plastic Films. *Nano Lett.* **2012**, *12*, 3109−3114.

(12) Wang, Z. L. Entropy Theory of Distributed Energy for Internet of Things. *Nano Energy* **2019**, *58*, 669−672.
(13) Zou, H.; Zhang, Y.; Guo, L.; Wang, P.; He, X.; Dai, G.; Zheng, H.; Chen, C.; Wang, A. C.; Xu, C.; Wang, Z. L. Quantifying the Triboelectric Series. *Nat. Commun.* **2019**, *10*, 1427.
(14) Wu, C.; Wang, A. C.; Ding, W.; Guo, H.; Wang, Z. L. Triboelectric Nanogenerator: A Foundation of the Energy for the New Era. *Adv. Energy Mater.* **2019**, *9*, 1802906.
(15) Wang, Z. L.; Wang, A. C. On the Origin of Contact-Electrification. *Mater. Today* **2019**, *30*, 34−51.
(16) Ye, J.; Cheng, Y.; Sun, L.; Ding, M.; Wu, C.; Yuan, D.; Zhao, X.; Xiang, C.; Jia, C. A Green SPEEK/Lignin Composite Membrane with High Ion Selectivity for Vanadium Redox Flow Battery. *J. Membr. Sci.* **2019**, *572*, 110−118.
(17) Ye, J.; Xia, L.; Wu, C.; Ding, M.; Jia, C.; Wang, Q. Redox Targeting-Based Flow Batteries. *J. Phys. D: Appl. Phys.* **2019**, *52*, 443001.
(18) Shao, L.; Zhou, L.; Yang, L.; Jia, C.; Wang, C.; Hu, S.; Zeng, X.; Yang, C.; Huang, C.; Zhou, Y. Enhanced 4.5V/55°C Cycling Performance of $LiCoO_2$ Cathode *Via* $LiAlO_2$-$LiCo_{1-x}Al_xO_2$ Double-Layer Coatings. *Electrochim. Acta* **2019**, *297*, 742−748.
(19) Zhang, C.; Tang, W.; Zhang, L.; Han, C.; Wang, Z. L. Contact Electrification Field-Effect Transistor. *ACS Nano* **2014**, *8*, 8702−8709.
(20) Gao, G.; Yu, J.; Yang, X.; Pang, Y.; Zhao, J.; Pan, C.; Sun, Q.; Wang, Z. L. Triboiontronic Transistor of MoS_2. *Adv. Mater.* **2019**, *31*, No. 1806905.
(21) Pang, Y.; Xue, F.; Wang, L.; Chen, J.; Luo, J.; Jiang, T.; Zhang, C.; Wang, Z. L. Tribotronic Enhanced Photoresponsivity of a MoS_2 Phototransistor. *Adv. Sci.* **2016**, *3*, 1500419.
(22) Gao, G.; Wan, B.; Liu, X.; Sun, Q.; Yang, X.; Wang, L.; Pan, C.; Wang, Z. L. Tunable Tribotronic Dual-Gate Logic Devices Based on 2D MoS_2 and Black Phosphorus. *Adv. Mater.* **2018**, *30*, 1705088.
(23) Li, J.; Zhang, C.; Duan, L.; Zhang, L. M.; Wang, L. D.; Dong, G. F.; Wang, Z. L. Flexible Organic Tribotronic Transistor Memory for a Visible and Wearable Touch Monitoring System. *Adv. Mater.* **2016**, *28*, 106−110.
(24) Xue, F.; Chen, L.; Wang, L.; Pang, Y.; Chen, J.; Zhang, C.; Wang, Z. L. MoS_2 Tribotronic Transistor for Smart Tactile Switch. *Adv. Funct. Mater.* **2016**, *26*, 2104−2109.
(25) Yang, Z. W.; Pang, Y.; Zhang, L.; Lu, C.; Chen, J.; Zhou, T.; Zhang, C.; Wang, Z. L. Tribotronic Transistor Array as an Active Tactile Sensing System. *ACS Nano* **2016**, *10*, 10912−10920.
(26) Khan, U.; Kim, T.-H.; Ryu, H.; Seung, W.; Kim, S.-W. Graphene Tribotronics for Electronic Skin and Touch Screen Applications. *Adv. Mater.* **2017**, *29*, 1603544.
(27) Chen, Y.; Gao, G.; Zhao, J.; Zhang, H.; Yu, J.; Yang, X.; Zhang, Q.; Zhang, W.; Xu, S.; Sun, J.; Meng, Y.; Sun, Q. Graphene Synapses: Piezotronic Graphene Artificial Sensory Synapse. *Adv. Funct. Mater.* **2019**, *29*, 1970286.
(28) Kong, L.-A.; Sun, J.; Qian, C.; Wang, C.; Yang, J.; Gao, Y. Spatially-Correlated Neuron Transistors with Ion-Gel Gating for Brain-Inspired Applications. *Org. Electron.* **2017**, *44*, 25−31.
(29) Kong, L.-A.; Sun, J.; Qian, C.; Gou, G.; He, Y.; Yang, J.; Gao, Y. Ion-Gel Gated Field-Effect Transistors with Solution-Processed Oxide Semiconductors for Bioinspired Artificial Synapses. *Org. Electron.* **2016**, *39*, 64−70.
(30) Sun, J.; Fu, Y.; Wan, Q. Organic Synaptic Devices for Neuromorphic Systems. *J. Phys. D: Appl. Phys.* **2018**, *51*, 314004.
(31) Meng, Y.; Zhao, J.; Yang, X.; Zhao, C.; Qin, S.; Cho, J. H.; Zhang, C.; Sun, Q.; Wang, Z. L. Mechanosensation-Active Matrix Based on Direct-Contact Tribotronic Planar Graphene Transistor Array. *ACS Nano* **2018**, *12*, 9381−9389.
(32) Kim, S.; Kim, Y. C.; Choi, Y. J.; Woo, H. J.; Song, Y. J.; Kang, M. S.; Lee, C.; Cho, J. H. Vertically Stacked CVD-Grown 2D Heterostructure for Wafer-Scale Electronics. *ACS Appl. Mater. Interfaces* **2019**, *11*, 35444−35450.
(33) Alquraishi, W.; Fu, Y.; Qiu, W.; Wang, J.; Chen, Y.; Kong, L.; Sun, J.; Gao, Y. Hybrid Optoelectronic Synaptic Functionality Realized with Ion Gel-Modulated In_2O_3 Phototransistors. *Org. Electron.* **2019**, *71*, 72−78.
(34) Sun, Q.; Ho, D. H.; Choi, Y.; Pan, C.; Kim, D. H.; Wang, Z. L.; Cho, J. H. Piezopotential-Programmed Multilevel Nonvolatile Memory As Triggered by Mechanical Stimuli. *ACS Nano* **2016**, *10*, 11037−11043.
(35) Yang, X.; Hu, G.; Gao, G.; Chen, X.; Sun, J.; Wan, B.; Zhang, Q.; Qin, S.; Zhang, W.; Pan, C.; Sun, Q.; Wang, Z. L. Coupled Ion-Gel Channel-Width Gating and Piezotronic Interface Gating in ZnO Nanowire Devices. *Adv. Funct. Mater.* **2019**, *29*, 1807837.
(36) Choi, Y.; Kang, J.; Jariwala, D.; Wells, S. A.; Kang, M. S.; Marks, T. J.; Hersam, M. C.; Cho, J. H. Low-Voltage 2D Material Field-Effect Transistors Enabled by Ion Gel Capacitive Coupling. *Chem. Mater.* **2017**, *29*, 4008−4013.
(37) Spijkman, M.-J.; Myny, K.; Smits, E. C. P.; Heremans, P.; Blom, P. W. M.; de Leeuw, D. M. Dual-Gate Thin-Film Transistors, Integrated Circuits and Sensors. *Adv. Mater.* **2011**, *23*, 3231−3242.
(38) Wang, Y. y.; Ni, Z. h.; Yu, T.; Shen, Z. X.; Wang, H. m.; Wu, Y. h.; Chen, W.; Shen Wee, A. T. Raman Studies of Monolayer Graphene: The Substrate Effect. *J. Phys. Chem. C* **2008**, *112*, 10637−10640.

https://dx.doi.org/10.1021/acsnano.9b09549
ACS Nano 2020, 14, 3461−3468